Journal of Applied Electrochemistry **34**: 1279–1285, 2004.

Fabrication of TiO_2 composite materials for air purification by magnetic field effect and electrocodeposition

S. YONEMOCHI[1,*], A. SUGIYAMA[2], K. KAWAMURA[1], T. NAGOYA[3] and R. AOGAKI[4]
[1]*Center for Environmental Science in Saitama, 914 Kamitanadare, Kisai-town, Saitama 347-0115, Japan*
[2]*Japan Society for the Promotion of Science, 1-6 Ichibancho, Chiyoda-ku, Tokyo 102-8471, Japan*
[3]*Waseda University, 3-4-1 Okubo, Shinjuku-ku, Tokyo 169-8555, Japan*
[4]*Polytechnic University, 4-4-1 Hashimotodai, Sagamihara, Kanagawa 229-1196, Japan*
*(*author for correspondence, Fax: +81-480-70-2031; e-mail: s-yonemochi@kankyou.pref.saitama.jp)*

Received 21 January 2004; accepted in revised form 14 July 2004

Key words: electrocodeposition, nitrogen oxides, magnetic field effect, photocatalyst, materials, titanium oxide

Abstract

Novel air purification materials were fabricated by the application of a magnetic field. In a magnetic field perpendicular to a copper plate, nickel particles with a diameter of 10 μm were arranged to form numerous pillar-like structures on the matrix surface, and copper as a binder was deposited onto the three-dimensional surface. The total surface area of the pillars and the matrix increased with the magnetic flux density, up to about 800 cm^2 per cm^2 of the original matrix surface at 6.2 T. After successful codeposition of TiO_2 particles on the fabricated materials by electroplating, their photocatalytic activities were evaluated on the basis of the removal efficiency of nitrogen oxides (NO_x), which are some of the most hazardous air pollutants. It was concluded that the samples with the pillar-like structures had two opposite characteristics: large surface area as a positive effect and shadowing against ultraviolet (UV) irradiation as a negative effect. However, total photocatalytic activity increased to twice as much as that of the flat sample by improving the UV irradiation method and the preparation condition of the materials.

1. Introduction

In 1972, Fujishima and Honda reported that water was decomposed into hydrogen and oxygen on the surface of TiO_2 under ultraviolet (UV) irradiation [1]. Thereafter, many researchers reported the applications of this reduction-oxidation system in various fields [2, 3]. Lately, TiO_2 has received considerable attention as one of the catalytic materials useful in the removal of pollutants [4]. However, for the practical application of photocatalysts like TiO_2 to air purification, it is necessary to fix them on solid matrices. The efficiency of the catalyst often changes with the matrices; therefore, the work of many researchers is focused on discovering better materials for the matrices [5–7]. The surface shape of the matrices is also important. Catalytic efficiency is expected to improve if surfaces with suitable shapes that support effective reaction are produced.

On the other hand, owing to recent developments in superconducting magnets, there has been an enhancement in the application of high magnetic fields to material processing. Material processing applied to (magnetohydrodynamics) (MHD) or micro-MHD effects is newly developing as magneto-electrolysis and magneto-plating. The MHD and micro-MHD effects imply the following phenomena. In electrochemistry, the reaction rates are greatly influenced by the fluid motions (referred to as MHD and micro-MHD flows) arising from the Lorentz force, and these motions accelerate or decelerate depending on the type of reaction [8, 9].

In magneto-plating, it has been reported that a variety of deposition surface shapes are produced by changing the direction of the magnetic field imposed on the electrodes. In a parallel magnetic field, where magnetic force lines are parallel to the electrode surface, crystal grains decrease in size and a flat surface is obtained [10]. In a vertical magnetic field, where magnetic force lines are placed perpendicular to the electrode surface, the deposition surface undergoes local suppression. Therefore, patterned micro holes emerge [11, 12]. Yamada and Asai [13] conducted nickel electroplating codeposited with Al_2O_3 particles in the vertical magnetic field and found that the Al_2O_3 particles were included in the nickel matrix in a regular pattern. All these results can be explained by the non-equilibrium fluctuation theory for electrodeposition in a magnetic field [9, 10].

With regard to the fixation of TiO_2 particles by composite plating, codeposition of Zn–TiO_2 [14] and Ni–TiO_2 [15] on a flat surface have been reported.

In this work, an attempt is made to form a matrix with a special steric structure using a magnetic field in order to enlarge the surface area of the matrix. The

codeposition of TiO_2 particles on the steric structure is also attempted by applying electroplating. The overall catalytic efficiency of the fixed TiO_2 particles was evaluated by the NO_x removal rate under UV irradiation.

2. Experimental details

2.1. *Production of catalytic material*

2.1.1. *General*

To fix TiO_2 particles on a base material, copper plating, which has high current efficiency and deposits fine crystals, was selected. Firstly, a copper plate was placed at the bottom of an electrolysis cell, and nickel particles were arranged to form numerous pillar-like structures in the vertical magnetic field. This procedure is the application of a simple and typical magnetic effect that orders ferromagnetic materials, such as iron and nickel particles, along magnetic force lines. Then, the cell was filled with a copper sulfate solution containing TiO_2 particles, and copper electrodeposition onto the copper plate with the pillar-like structures of nickel particles was conducted in the vertical magnetic field. It was expected that a series of these procedures would produce a special copper plate with minute pillar-like structures, covered with copper and TiO_2 particles as shown in Figure 1.

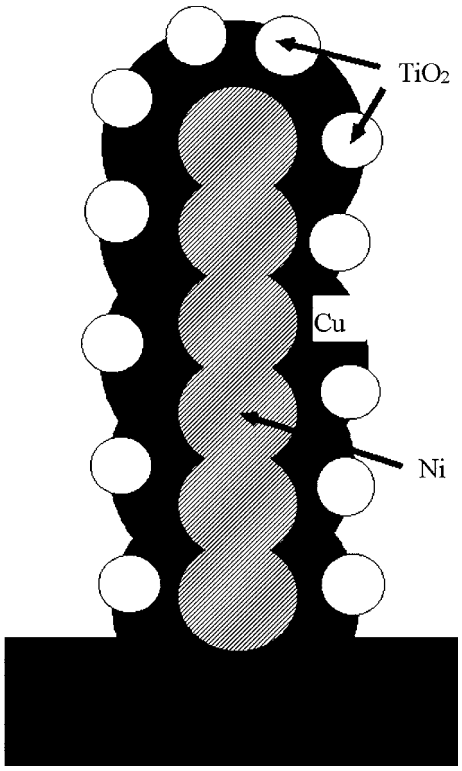

Fig. 1. Schematic figure of a pillar-like structure produced by ordered nickel particles with copper and TiO_2 particle.

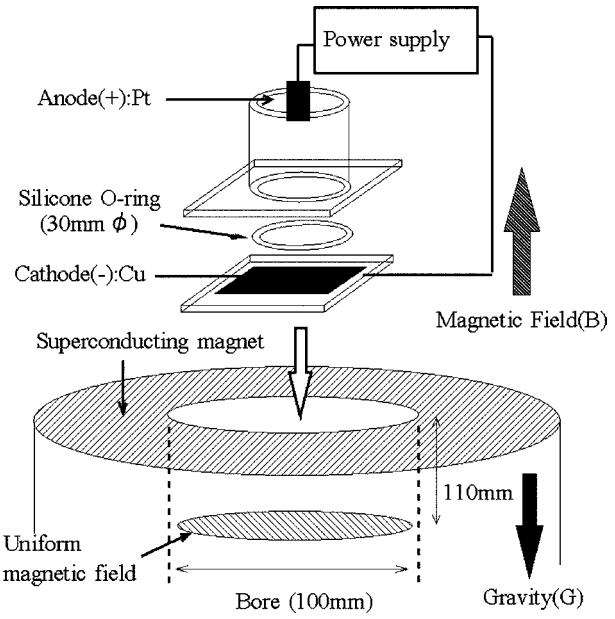

Fig. 2. Schematic configuration of the electrolysis cell.

2.1.2. *Electrolysis cell*

Figure 2 exhibits the schematic configuration of the electrolysis cell used for the production of matrices. A copper plate was placed as a working electrode at the bottom of the cell made of acrylic resin, and a silicone O-ring with a diameter of 30 mm was placed on the plate. Two types of platinum plate with a thickness of 0.1 mm were used as counter electrodes: one was a rectangular plate with dimensions of 10 mm × 30 mm with both sides being used as the working area, and the other was a round plate with a diameter of 27.6 mm and only one side being used as the working area. Both the electrodes had the same working areas with either plate being placed over the working electrode. The surface of the counter electrode to the copper plate was perpendicular to the former plate and parallel to the latter plate.

2.1.3. *Application of a magnetic field*

For the experiments conducted under a low magnetic field, a ferrite magnet with dimensions of 40 mm × 40 mm × 10 mm and an average magnetic flux density was 0.043 T was used. To generate a high magnetic field, a liquid-helium-free superconducting magnet (HF10-100VHT, Sumitomo Heavy Industries, Ltd.) was utilized; the bore diameter was 100 mm, and a magnetic flux density of up to 10 T could be imposed.

The electrolysis cell was placed either on the permanent magnet or in the bore space of the superconducting magnet. The magnetic flux density depended on the position in the bore space. Therefore, a uniform magnetic field, which existed 110 mm below the upper face of the superconducting magnet (see Figuer 3), was selected to stack nickel particles vertically on a copper plate. Further, a magnetic flux density of up to 6.2 T could be imposed at its position in the bore space. Electroplating was carried out in the magnetic field of a

superconducting magnet at 0.6, 3.1 and 6.2 T, and of a ferrite magnet at 0.043 T.

2.1.4. *Plating conditions*

To apply magneto-plating to the fabrication of photocatalyst matrices containing TiO_2 particles, fundamental plating conditions, such as TiO_2 concentration, current density, and the magnetic flux density were examined without nickel particles. An electrolyte solution of 20 ml that contained 1.0 mol dm^{-3} of copper sulfate was mixed with TiO_2 particles with a diameter of 7 nm (anatase, ST-01, Ishihara Sangyo, Ltd.), the amount of which was changed from 0.015 to 0.3 g.

Usually, when copper electroplating is carried out with copper sulfate solution under galvanostatic conditions, a mixture of copper sulfate and sulfuric acid, which functions as the supporting electrolyte, is used as the electrolysis solution. However, only a few TiO_2 particles were codeposited in the presence of sulfuric acid. Therefore, the solution without sulfuric acid was chosen as the plating solution.

After the cell was filled with the plating solution in the magnetic field, electroplating onto the copper plate (working electrode) was performed at a constant current density of 16.7 A dm^{-2} for 30 min or 8.4 A dm^{-2} for 60 min with a potentio-galvanostat (PS-14, Tohogiken, Ltd.), at room temperature.

2.1.5. *Formation of the pillar-like structures*

To form the pillar-like structures, 0.2 g of nickel particles 10 μm in diameter were spread directly over the copper plate without the plating solution in the vertical magnetic field. The plating conditions were the same as mentioned above.

2.2. *Characterization of materials*

Observation of material surface and measurement of the TiO_2 codeposition ratio on the surface were carried out with a scanning electron microscope equipped with an energy-dispersive X-ray spectroscopy detector (SEM-EDX Type-N, Hitachi, Ltd.). The surface areas of the samples were measured by the Brunauer–Emmett–Teller (BET) method, using a specific surface area measurement system (ASAP 2010, Shimazu, Ltd.).

2.3. *Evaluation of catalysis activities*

Figure 3 is the schematic illustration of the reactor, which had a volume of 0.194 m^3 and was used to evaluate catalysis activities by NO_x removal. Two lamps and two sheets of aluminum foil could be attached under the upper tray. Usually, only a single lamp without aluminum foil is used. Two fans were set in the reactor to establish uniform gas concentration. The lower tray could be moved in the vertical direction to adjust the intensity of light. The fabricated sample was set on the lower tray and NO gas with a concentration of 1.0 ppm was introduced. After irradiating the sample

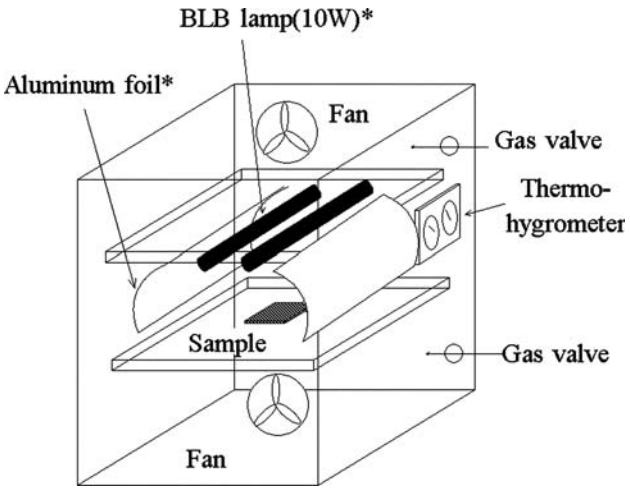

Fig. 3. Schematic illustration of the reactor. * Irradiation with a single lamp without aluminum foil is the usual condition.

with UV rays (365 nm, 2.0 mW cm^{-2}) for 1 h with a 10 W BLB-Lamp (FL10BLB-A, Toshiba, Ltd.) and without aluminum foils, which are a part of the usual experimental condition, the sample was dipped in 10 ml pure water for 1 h. NO_2^- and NO_3^- eluted in the water were analyzed by an ion- chromatograph (IC-20, Dionex, Ltd.), and the amount of NO_2 produced in the residual gas was determined by the Salzmann method [16].

3. Results and discussion

3.1. *Characteristics of the pillar-like structures*

TiO_2 composite materials with the pillar-like structures are shown in Figure 4. Remarkable success was achieved in arranging the nickel particles that formed the pillar-like structures. In Figure 5, the maximum length and the number density of the pillars are plotted against the magnetic flux density. As the magnetic flux density increased, pillar sizes decreased and their number density increased on the contrary; it attained a maximum pillar size of 2 mm and 1200 counts per cm^2 in terms of number density of the pillars at 6.2 T. Total surface area also increased with the number density, and it attained 800 cm^2 per cm^2 of the original matrix surface at 6.2 T.

3.2. *Codeposition of TiO_2*

Figure 6 shows the TiO_2 codeposition ratio, which is defined as the weight of TiO_2 in the deposited surface, onto a flat surface in the vertical magnetic field. The ratio increased with an increase in the TiO_2 concentration in the plating solution and considerably decreased with an increase in the magnetic flux density, although the high magnetic flux density was effective in generating numerous pillars, as mentioned in 3.1. The effect of the magnetic field on TiO_2 codeposition was investigated in details as follows:

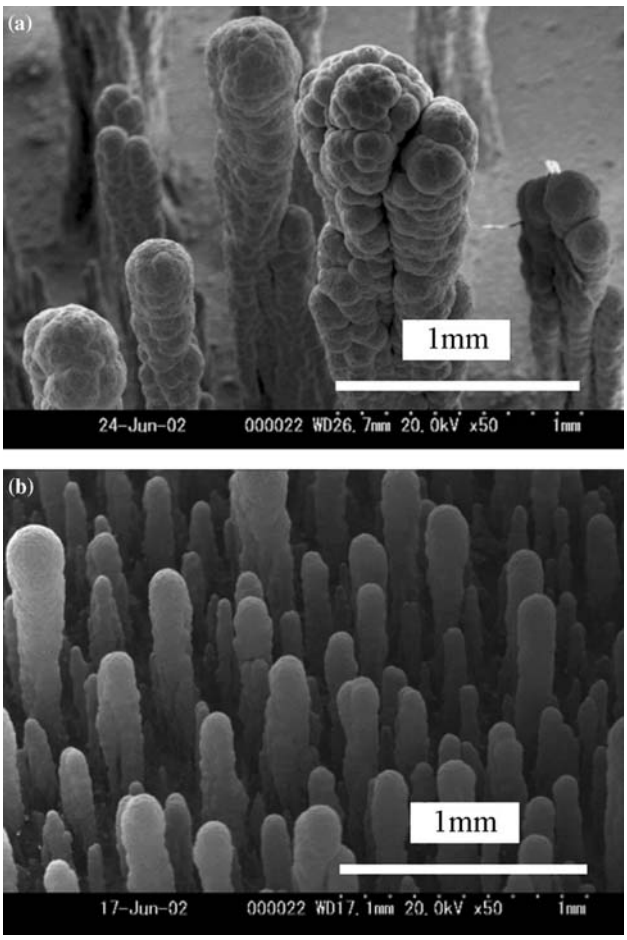

Fig. 4. SEM photographs of the pillar-like structures produced under low and high magnetic flux densities. (a) 0.043/T and (b) 6.2/T.

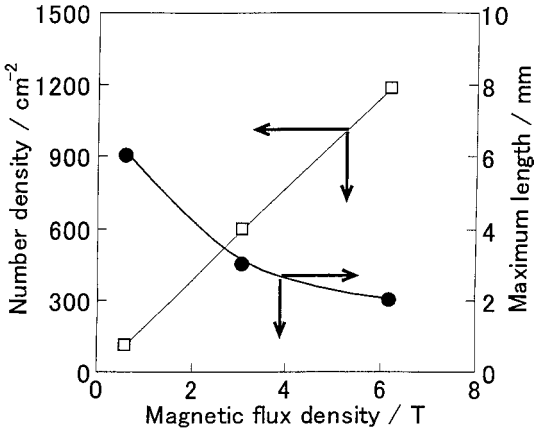

Fig. 5. Effects of the magnetic flux density on the number and size of the pillar-like structures.

Several mechanisms for codeposition of dispersed particles had been proposed [17–19]; one of the essential processes is to keep TiO_2 particles adsorbed on the electrode surface. The possible effects of the magnetic field on this process are: (1) adherence to the magnetic force and (2) solution flow such as the MHD and micro-MHD flows induced by magnetic force. However, as magnetic susceptibility of TiO_2 is negligibly small and is

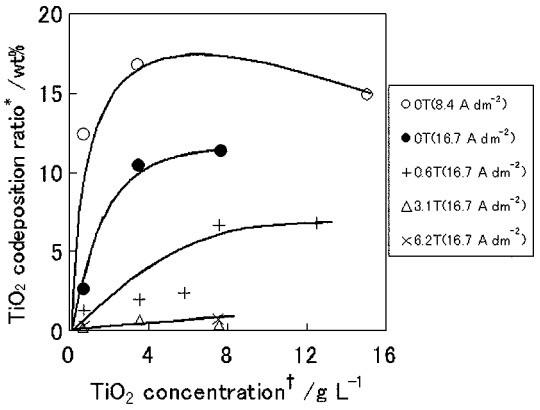

Fig. 6. TiO_2 codeposition ratio under various conditions. Current density of 16.7 A dm^{-2} was applied for 30 min or 8.4 A dm^{-2} for 60 min. *TiO_2 ratio in the deposited surface containing TiO_2 and copper. † Concentration in the plating solution.

$+5.9 \times 10^{-6}$ cm^3 mol^{-1} at room temperature [20], the magnetic force does not affect TiO_2 particles directly.

To evaluate the effect of the MHD and micro-MHD flows on the TiO_2 codeposition ratio, the surface direction of the counter electrode to the magnetic field was changed at 3.1 T by setting its direction parallel or vertical. As shown in Table 1, the ratio obtained in the vertical configuration was several times larger than that in the parallel configuration at each TiO_2 concentration. In the parallel configuration, the electrolytic current (i) had an orthogonal component (i_x) to the magnetic field direction as shown in Figure 7(a). Therefore, the MHD flow generated by the Lorentz force (F) proceeded on the electrode surface [9], and many minute vortices emerged above the surface [11]. On the contrary, in the vertical configuration shown in Figure 7(b), the MHD flow was weaker than the former.

To evaluate the effect of the strength of solution flow on the TiO_2 codeposition ratio, a series of experiments were conducted using a mechanical agitator with a rotor instead of the MHD flow, in the absence of a magnetic field. The ratio decreased with rotation speed. Figure 8 shows the results. This means that TiO_2 particles adsorbed on a matrix were stripped away by a rapid solution flow.

Table 1. Effects of the direction of anodes surface on TiO_2 codeposition ratio

TiO_2 concentration of plating bath/gl^{-1}	Anode direction to magnetic field	TiO_2 codeposition ratio/wt%
0.8	Parallel*	0.17
	Vertical†	0.55
3.5	Parallel	0.70
	Vertical	2.99
7.5	Parallel	0.35
	Vertical	1.30

*Shown in Figure 7(a). †Shown in Figure 7(b). A current density of 8.4 A dm^{-2} was applied for 60 min and the magnetic flux density was 3.1 T.

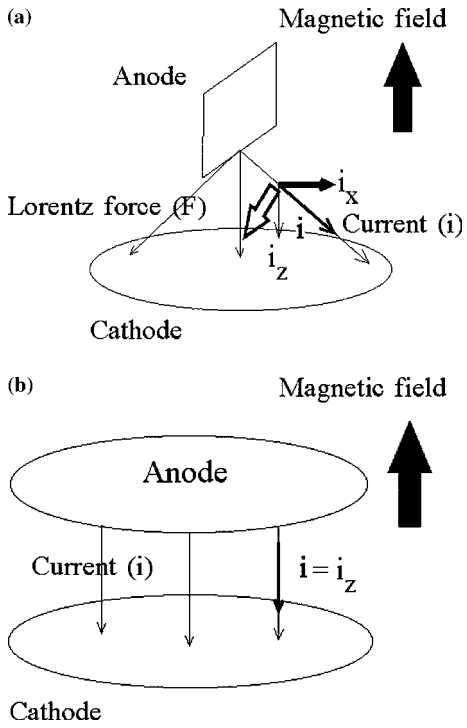

Fig. 7. Schematic figures of the relationship between electrode configuration and the Lorentz force. (a) Parallel configuration and (b) Vertical configuration.

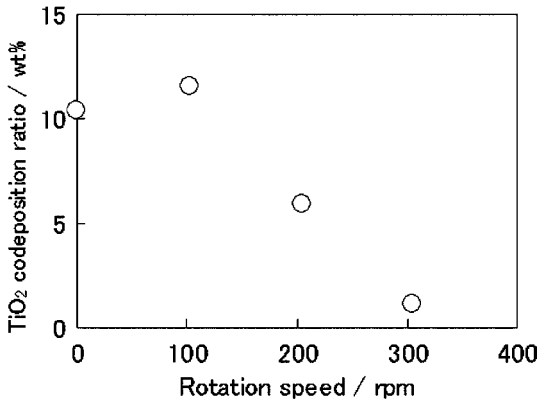

Fig. 8. Effects of rotation speed on the TiO_2 codeposition ratio in the absence of a magnetic field. 0.07 g of TiO_2 was dispersed in 20 ml of 1 mol dm^{-3} $CuSO_4$ solution.

Based on these results, it can be deduced that TiO_2 barely codeposited in a high magnetic field for the following reason. Although adsorption of TiO_2 particles on a matrix surface was required for codeposition, almost all TiO_2 particles adsorbed on the electrode surface were stripped by the MHD and micro-MHD flow.

3.3. *Improvement of preparation procedures*

Considering these results, two sequential processes were employed in an attempt to fabricate TiO_2 composite materials. At first, the pillar-like structures were prepared in a high magnetic field. Then, TiO_2 particles were codeposited in the absence of a magnetic field. As a result, TiO_2 particles were fixed successfully onto the pillars and flat-bottom surfaces. TiO_2 codeposition ratios on the top surface of the pillars and the bottom surface were around 5 wt% and around 15 wt%, respectively, under the following conditions: (1) 8.4 A dm^{-2} for 60 min at 6.2 T during the first step, and (2) 0.07 g of TiO_2 with 8.4 A dm^{-2} for 60 min in the absence of a magnetic field during the second step.

Further, the plating condition was examined from the point of view of increasing the TiO_2 ratio of the top surface. Changing the anode direction and the addition of 0.5 mol dm^{-3} sulfuric acid, which caused the change in current distribution, were tried for this purpose. Table 2 shows the results and suggests that these operations can control the TiO_2 codeposition ratio on the steric surface.

3.4. *Evaluation of catalytic efficiency*

The catalytic efficiencies of the flat samples are shown in Figure 9. The main products were NO_2, NO_2^-, and NO_3^-. Generally speaking, NO_x refers to both NO and

Table 2. Changes of amount of TiO_2 codepositon ratio. Current density of 8.4 A dm^{-2} was applied for 60 min

Condition		Amount of TiO_2 codeposition	
Anode direction to magnectic field	Sulfuric acid /mol dm^{-3}	Bottom surface /wt%	Top of pillar /wt%
Parallel	0	12.8	2.5
Vertical	0.5	2.0	13.1

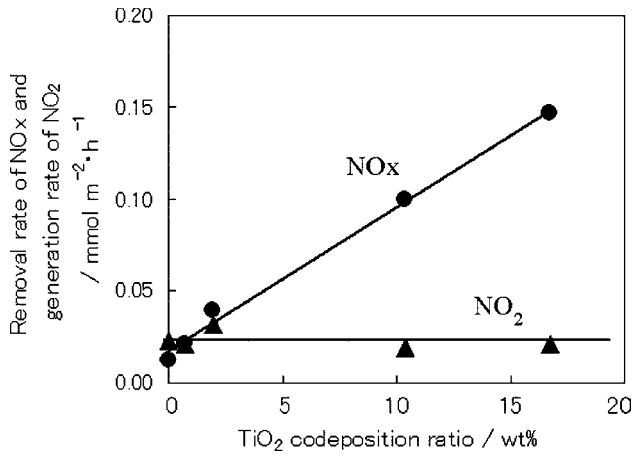

Fig. 9. Photocatalytic activities of the prepared samples. UV irradiation of 2.0 mW cm^{-2} at 365 nm was conducted for an hour at room temperature.

NO_2; therefore, NO_x removal rate was defined as the generation rate of NO_3^- and NO_2^- on the sample surface. As shown in Figure 9, NO_x removal rate increased linearly with the TiO_2 ratio. The relationship between NO_x removal rate (r) and TiO_2 codeposition ratio (c) was expressed by the following equation.

$$r = 0.0078c + 0.0171 \quad (1)$$

This implies that the efficiency is related only to the TiO_2 ratio in the case of flat samples, and nitrogen oxide is partially oxidized to nitric acid without TiO_2 by oxygen or activated oxygen species generated under UV irradiation.

At the same time, generation rate of NO_2, which is more hazardous than NO and an oxidized form of NO, was almost constant. Usually, NO is oxidized to NO_3^- through the formation of NO_2, which is not strongly adsorbed on TiO_2. Therefore, the NO_2 generation rate usually increases undesirably with oxidation progress on the TiO_2 surface. However, in the case of this material, the NO_2 generation rate was almost the same as that of a copper plate used for the blank examination. The mechanism of this effect was under investigation.

In addition, the NO_x removal rates of some samples with the pillar-like structures prepared under 6.2 T were evaluated under the same experimental conditions as the flat samples in term of UV strength, irradiation times and initial NO concentration. The dependence of the NO_x removal rate on the TiO_2 codeposition ratio of the pillar top surface is shown in Table 3. The removal rates increased with the TiO_2 codeposition ratio of the pillar top surface, independent of those of the bottom surface. It is reasonable because the pillar top surface was exposed efficiently to UV rays, compared with the other parts such as the bottom. However, the total numbers of activities were less than those of the corresponding flat samples. The presence of numerous pillars resulted in a drastic increase in the surface area, simultaneously generating a shadowed area when irradiated with UV rays, where the photocatalyst was not activated.

Table 3. NO_x removal rate of pillar-like structure

TiO_2 codepositon ratio/wt%		NOx removal rate/mmol m^{-2} h^{-1}
Top of pillar	Bottom surface	
0	0	0.012*
3.5	13.9	0.023
8.4	9.0	0.037
17.4	2.2	0.048

*Only UV irradiation without a sample. All the conditions were the same as those applied to the experiments in Figure 9.

Figure 10 compares the NO_x removal rates of samples with pillars and those of the flat samples. In the case of the samples with the pillars, the removal rates were corrected by dividing them by a ratio of the total surface area of the pillar top surface to that of the base material, based on the assumption that NO_x was removed only on the pillar top surface. These values were defined as the corrected NO_x removal rates on the horizontal axis. The area ratio was calculated using SEM image data and was 0.345 on an average. The NO_x removal rates of the flat samples were calculated by substituting the TiO_2 codeposition ratio of the pillar top surface in Equation (1), and these values are defined as the expected NO_x removal rate on the vertical axis. Both the values were approximately the same. At the same time, it could be concluded that, on the bottom surface, only a few photocatalysts were activated.

To check this assumption, additional examinations were carried out by using irradiation with double lamps to strengthen the intensity of light and aluminum foil walls to scatter the direction of light (see Figure 3).

As shown in Table 4, NO_x removal rates of the samples with the pillar-like structures increased as expected. In particular, in the case of the sample with 3.5 wt% on the pillar top surface and 13.9 wt% on the bottom surface in the TiO_2 codeposition ratio, removal

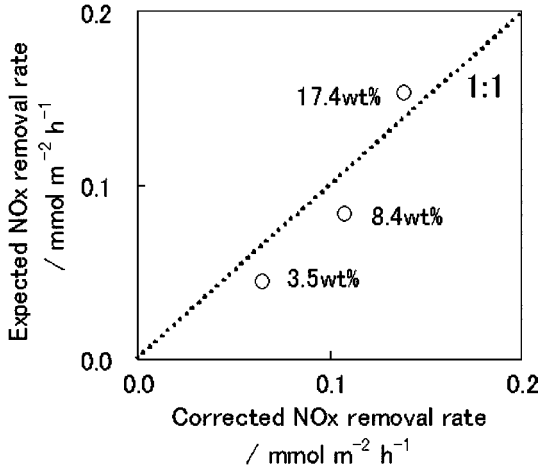

Fig. 10. Comparison of corrected and expected NO_x removal rates. Weight percentages in the figure show the TiO_2 codeposition ratio on the pillars' top surface. The other conditions were the same as those applied to the experiments in Figure 9.

Table 4. NO_x removal rate of pillar-like stucture (2)

TiO_2 codeposition ratio/ wt%		NO_x removal rate/ mmol m^{-2} h^{-1}	
Top of pillar	Bottom surface	Single lamp	Double lamps and aluminium foils
3.5	13.9	0.023	0.119
17.4	2.2	0.048	0.085
–	16.8*	0.146	0.135

*Flat shape without pillars. The conditions were the same as those for the experiments in Figure 9, except for UV irradiation.

Table 5. Effects of pillar density on NO_x removal rate

TiO_2 codeposition ratio/ wt%		Pillar density/ count cm^{-2}	NO_x removal rate/ mmol m^{-2} h^{-1}
Top of pillar	Bottom surface		
3.5	14.5	108	0.220
5.6	16.7	134	0.285
3.5	13.9	1210	0.119
–	16.8*	–	0.135

*Flat shape without pillars. Irradiation was conducted with double BLB lamps and aluminum foils. The other conditions were the same as those for the experiments in Figure 9.

rate increased fivefold, though that of the flat sample as the reference did not change to such an extent. However, even the maximum removal rate of the pillar-like structures was lower than that of the flat sample. It was speculated that the pillar density was too high. If the magnetic flux density was decreased when preparing the pillars, the pillar density could be lowered, even though the length of the pillar would, unfortunately, increase at the same time. To suppress the length of the pillar, 0.1 g of nickel particles were applied. The effect of pillar density on NO_x removal rate is shown in Table 5. The pillar density prepared under 0.6 T, was about one-tenth of that prepared under 6.2 T, and the pillar length was kept at a maximum of 3 mm. The removal rate increased successfully to 0.220 and 0.285 mmol m^{-2} h^{-1}, which were twice as much as that of the flat sample or that of the high pillar density. It was explained that TiO_2 on the bottom surface and the side of the pillar was activated with a decrease in the shadowed !area. Therefore, it was expected that NO_x removal rates of the samples with the pillar-like structures could increase further by optimizing the pillar density and size and modifying the irradiation equipment and methods.

4. Conclusions

TiO_2 composite materials with a three-dimensional surface of a quite new type were produced for application to air purification. The magnetic field played two different roles on catalytic efficiencies: a negative effect of decreasing TiO_2 codeposition ratio, and a positive effect of increasing surface area. These effects contradicted each other. Therefore, to codeposit many TiO_2 particles onto the steric surface, a preparation method with two plating steps was proposed. At the same time, the plating conditions for TiO_2 codeposition onto the pillars' top surface were determined.

The NO_x removal rate was examined with a view to its application to air purification. In the cases of flat samples, the NO_x removal rate increased with the TiO_2 codeposition ratio. On the other hand, in the case of the pillar samples, the NO_x removal rate was lower than that of the corresponding flat sample under the same irradiation condition. Modifying irradiation conditions and decreasing pillar density successfully improved the NO_x removal rates. Therefore, catalytic activity can be further increased by optimizing the UV irradiation methods and pillar density.

Acknowledgements

The authors wish to acknowledge the helpful discussions with Mr. Y. Nagai, Mr. M. Hashiride and Mr. R. Morimoto, and thank Saitama Industry Technology Center for permitting the use of their superconducting magnet and other apparatus.

References

1. A. Fujishima and K. Honda, *Nature* **238** (1972) 5358.
2. R. Wang, K. Hashimoto, A. Fujishima, M. Chikuni, E. Kojima, A. Kitamura, M. Shimohigoshi and T. Watanabe, *Nature* **388** (1997) 431.
3. B. Krauetler and A.J. Bard, J. *Am. Chem. Soc.* **100** (1978) 5985.
4. K. Takeuchi and T. Ibusuki, *Atmos. Environ.* **20** (1986) 1155.
5. K. Takeuchi and T. Ibusuki, *J. NIRE* **3** (1994) 103.
6. T. Nonami, H. Taoda, N.T. Hue, E. Watanabe, K. Iseda, M. Tazawa and M. Fukaya, *Mat. Res. Bull.* **33** (1998) 125.
7. Y. Tonegawa, K. Sekiguchi, K. Nomura and K. Sakamoto, J. Jpn. *Soc. Atoms. Environ.* **38** (2003) 227.
8. M. Asanuma and R. Aogaki, *in* P.L. Bonora and F. Deflorian (eds), *Electrochemical Approach To Selected Corrosion and Corrosion Control Studies*, (IOM Communications, Great Britain, 2000) p. 310.
9. R. Aogaki, *Proc. of Symosium on New Magneto-Science 2000*, (NRLM-JST, Omiya, 2001) p. 27.
10. R. Morimoto, M. Hashiride, Y. Nagai, A. Sugiyama and R. Aogaki, *Surface Finish. Soc. Jpn.* **53** (2002) 453.
11. R. Aogaki and A. Sugiyama, *Proc. of Symposium on New Magneto-Science 2002*, (NIMS, Tsukuba, 2002) p. 136.
12. S. Yonemchi, T. Iwasaka and R. Aogaki, *Surface Finish. Soc. Jpn.* **50** (1999) 1015.
13. T. Yamada and S. Asai, *J. Jpn Inst. Metals* **65** (2001) 910.
14. T. Deguchi, K. Imai, M, Izasaki, H. Tada and S. Ito, *J. Electrochem. Soc.* **147** (2000) 2263.
15. N.R. de Tacconi, K. Carmona and K. Rajeshwar, *J. Phys. Chem. B.* **101** (1997) 10151.
16. JIS (Japanese Industrial Standard) K 0104.
17. N. Guglielmi, *J. Electrochem. Soc.* **119** (1972) 1009.
18. A.M.J. Kariapper and J. Foster, *Trans. Inst. Metal Finish.* **52** (1974) 87.
19. J.P. Celis, J.R. Roos and C. Buelens, *J. Electrochem. Soc.* **134** (1987) 1402.
20. D.R. Lide (ed.), Handbook of Chemistry and Physics, 71st edn. (CRC press, 1990) pp. 4–138.